CrystEngComm

www.rsc.org/crystengcomm

Volume 14 | Number 6 | 21 March 2012 | Pages 1887–2334

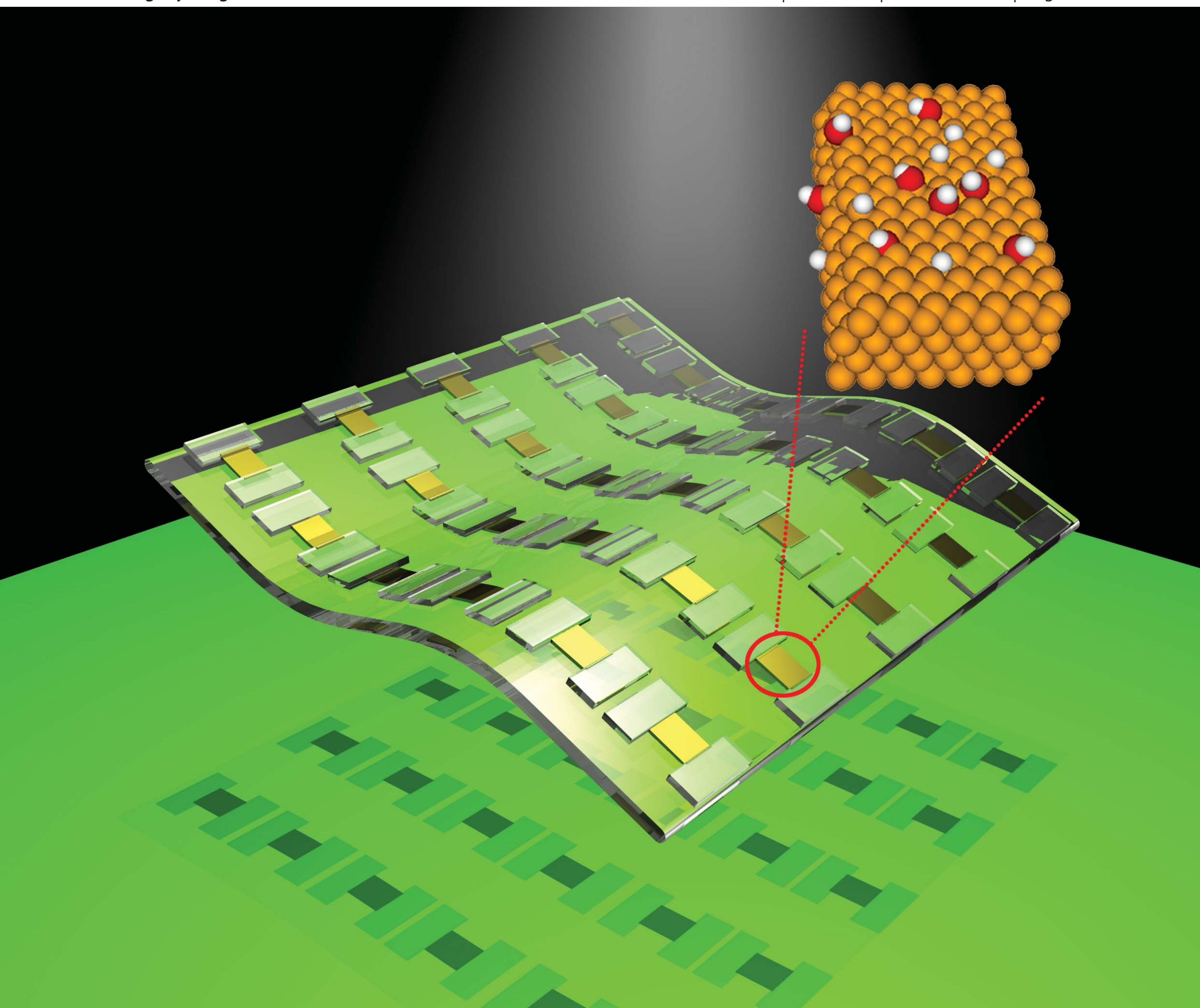

RSC Publishing

COVER ARTICLE

Luo *et al*.

Transparent and flexible selenium nanobelt-based visible light photodetector

CrystEngComm

Dynamic Article Links

Cite this: *CrystEngComm*, 2012, **14**, 1942

www.rsc.org/crystengcomm

PAPER

Published on 23 January 2012. Downloaded by HeFei University of Technology on 18/10/2015 13:16:02.

Transparent and flexible selenium nanobelt-based visible light photodetector

Lin-Bao Luo,*[a] Xiao-Bao Yang,*[b] Feng-Xia Liang,[c] Jian-Sheng Jie,*[a] Qiang Li,[a] Zhi-Feng Zhu,[a] Chun-Yan Wu,[a] Yong-Qiang Yu[a] and Li Wang[a]

Received 25th October 2011, Accepted 6th December 2011
DOI: 10.1039/c2ce06420k

We report a synthesis of single-crystal [001] oriented selenium nanobelts (SeNBs) through a simple vacuum evaporation at 250 °C. The width and thickness of the SeNBs are in the range of 100–800 nm and 20–90 nm, respectively. *I–V* analysis of an individual SeNB based field effect transistor (FET) reveals typical p-type electrical conduction. The hole mobility and concentration are respectively estimated to 0.63 $cm^2 (V s)^{-1}$ and 9.35×10^{16} cm^{-3}. The p-type electrical characteristics can be explained by the surface termination model, according to which, H- or OH- termination can induce a defect level slightly above the valance band maximum (VBM). A fully transparent and flexible visible light photodetector assembled on a polyethylene terephthalate (PET) substrate shows a high sensitivity to visible light illumination, with sensitivity and conductive gain as high as 3.27×10^4 A W^{-1} and 6.77×10^4 respectively. Furthermore, the device also exhibits a stable performance and good reproducibility under different bending conditions. The high-performance visible light photodetector would enable application opportunities in future flexible and transparent electronics.

Introduction

Selenium is known as an important trace element for humans owing to its nutritional effects in biology. For instance, it can function as a cofactor for reduction of antioxidant enzymes including glutathione peroxidases and thioredoxin reductase.[1] Selenium attracts even more research interest in both material and physics sciences by virtue of its novel properties, such as low melting point (217 °C), large birefringence, high photoconductivity (8×10^4 S cm^{-1}), large piezoelectric, thermoelectric, and non-linear optical response.[2] Commercial products that depend on selenium include photographic recording media, flat panel X-ray image detectors, Xerography, photoelectric cell, pressure sensors, *etc.*[3]

Like other photonic semiconductors, when the size and dimension shrink to the nanoscale level, selenium nanostructures in a one-dimensional (1-D) form (*e.g.*, nanorods, nanowires, nanobelts and nanotubes) are expected to exhibit a quantum-size effect which might bring out improved physical, catalytic and optical properties and therefore induce new applications in photonic devices.[4] By this token, a great number of methods have been developed to synthesize various 1-D nanostructures over the past decade. Xia and co-workers reported the fabrication of Se nanowires (SeNWs) by aging amorphous selenium colloids in the dark.[5] Lu *et al.* demonstrated the formation of Se nanobelts (SeNBs) by using cellulose as both the reducing and morphology-directing agents under hydrothermal conditions.[6] Liu and Li fabricated SeNWs through a "solid–solution–solid" growth process by dispersing Se spheres in ethanol.[7] Generally, the Se nanostructures obtained from the above solution based techniques are not good candidates for device application in that these nanostructures are usually characterized by poor crystallinity, surfactants absorption, and abundance of large quantity of defects, which will greatly restrict carrier transportation. On the other hand, the synthetic process normally involves the unfavorable chemical reduction of toxic H_2SeO_3 (SeO_2) or Na_2SeO_3 which are not environmentally benign.[8–10] Herein we report a synthesis of SeNBs by a simple thermal evaporation method. The high quality single crystal SeNBs show an oriented growth direction along [001]. *I–V* analysis of a single SeNB based field effect transistor (FET) reveals typical p-type conduction behavior. A photodetector made from individual SeNB exhibits a high light on–off current ratio of 1000. The responsivity and photoconductive gain is estimated to be 3.27×10^4 A W^{-1} and 6.77×10^4, respectively. What is more, the device can work under bending conditions with excellent reproducibility and stability. These results corroborate that the p-type SeNBs obtained *via* thermal evaporation are promising building blocks for nano-optoelectronic devices application.

[a]*School of Electronic Science and Applied Physics, Hefei University of Technology, Hefei, Anhui, 230009, P. R. China. E-mail: luolb@hfut.edu.cn; jsjie@hfut.edu.cn*
[b]*Department of Physics, South China University of Technology, Guangzhou, 510641, Guangdong Province, P. R. China. E-mail: scxbyang@scut.edu.cn*
[c]*Department of Physics and Materials Science, City University of Hong Kong, Kowloon, Hong Kong SAR, P. R. China*

Experimental

Synthesis and characterization of SeNBs

The fabrication of SeNBs was carried out in a tube furnace. Briefly, selenium powder (analytical grade, Sigma-Aldrich Co.)

 This journal is © The Royal Society of Chemistry 2012

Published on 23 January 2012. Downloaded by HeFei University of Technology on 18/10/2015 13:16:02.

was placed at the center of an alumina tube, silicon substrates were placed at the downstream position of the source material. After the tube was evacuated to a base pressure of 10^{-4} Torr, the source was heated up to 250 °C at a rate of 5 °C min^{-1} and maintained at this temperature for 1 h. During the growth process, a carrier gas of high-purity argon was fed at a total flow rate of 10 Sccm. The morphology, chemical composition and crystal structure of SeNBs were examined by X-ray diffraction (XRD), scanning electron microscopy (SEM, Philips XL 30 FEG), energy-dispersive X-ray spectroscopy (EDX), transmission electron microscopy (TEM, Philips CM 20, operating at 200 kV) and high-resolution transmission electron microscopy (HRTEM, CM 200 FEG operating at 200 kV). It should be noted that the SeNBs were ground by an agate mortar prior to XRD powder analysis. Raman analysis was conducted with a Renishaw 2000 laser Raman microscope equipped with a 633 nm argon ion laser of 2 μm spot size for excitation. The UV-vis absorption spectrum was performed using a spectrometer (Perkin Elemer, Lambda 2S).

Device fabrication and characterization

To fabricate a single SeNB-FET, the as-colleted NBs were first dispersed in ethanol, and then spread on a SiO_2 (500 nm)/p^+-Si substrate at a desired density. A photolithography technique and electron beam evaporator were then used to define both the source and drain electrodes. The preparation of a transparent and flexible photodetector is largely similar to the SeNB-FET except the substrate and electrode material. Typically, NBs were dispersed on a clean polyethylene terephthalate (PET) substrate, followed by the definition of the transparent source and drain electrode. An indium doped tin oxide (ITO) thin film was deposited using a magnetron sputtering system. The measurements of the SeNBs based field effect transistor and photodetectors were performed on the semiconductor characterization system (4200-SCS, Keithley Co.) with picoampere resolution. A light system including a Xenon lamp (150 W) and a monochromator (1/8, Spectro-physics 74000) was employed to provide the monochromatic light, which was focused and guided on the SeNB based device by a quartz lens.

Theoretical simulation

The theoretical modeling is based on the density functional theory (DFT) calculations, implemented in the VASP method. The energy cutoff is set to be 400 eV and the GGA-PW91 exchange–correlation functional is used. The distance between SeNWs in neighboring supercells is over 9 Å, which is large enough to eliminate cell-to-cell interactions. We adopted the Monkhorst–Pack sampling with a 1 × 1 × 4 k-point grid for the optimization of SeNWs, which is 1 × 1 × 10 for the band structures' calculation. Using the conjugate gradient method, we fully optimized both the atomic configurations and the lattice constant of all models, with the force criteria set at 0.01 eV $Å^{-1}$.

Results and discussion

The fabrication of the SeNBs was carried out in a three-temperature zone tube furnace. Pure Se powder and Si substrate were placed in two adjacent zones, whose temperatures can be tuned individually and precisely. Fig. 1(a) displays a typical XRD pattern of the product. All of the strong peaks can be readily indexed to trigonal selenium in which infinite helical chains of selenium atoms are packed parallel to each other along the *c*-axis. The lattice constants calculated from the diffraction pattern are a = 4.37 Å and c = 4.96 Å, which are in good agreement with both standard (JCPDS File No. 06-0362) and literature values.[11,12] The as-prepared SeNBs were directly transferred into a SEM chamber for morphology study. Fig. 1(b), (c), (d) and (e) show typical SEM images of the SeNBs at different magnifications. The width and thickness of the NBs are in the range of 100–800 nm and 20–90 nm, respectively. Moreover, the surfaces of the belts are smooth and clean, and each belt is relatively uniform throughout the length. The typical length of the NBs is about 20–40 μm. The SAED pattern and HRTEM image reveal the single-crystal nature of the NBs and growth direction of [001], consistent with the literature value.[13] The EDS spectrum in Fig. 2(b) shows only Se and Cu peaks (Cu signal comes from the TEM grid). In fact, the trigonal selenium phase was also confirmed by μ-Raman analysis shown in Fig. 2 (c). The strong Raman resonance peak at 235 cm^{-1} is a characteristic stretching mode of a chain-like structure that only exists in trigonal selenium.[14] The peak at 145 cm^{-1} is attributed to the transverse optical phonon mode.[15]

A FET based on an individual SeNB was fabricated to examine its transport properties. The inset in Fig. 3(a) displays a representative device in which two parallel Ti/Au (2/78 nm) electrodes are connected by a single SeNB with width of ∼500 nm. Fig. 3(b) shows the source–drain current (I_{ds}) *versus* source–drain voltage (V_{ds}) relations measured at various gate voltages (V_{gs}). It can be found that for all V_g, I_{ds} increases with

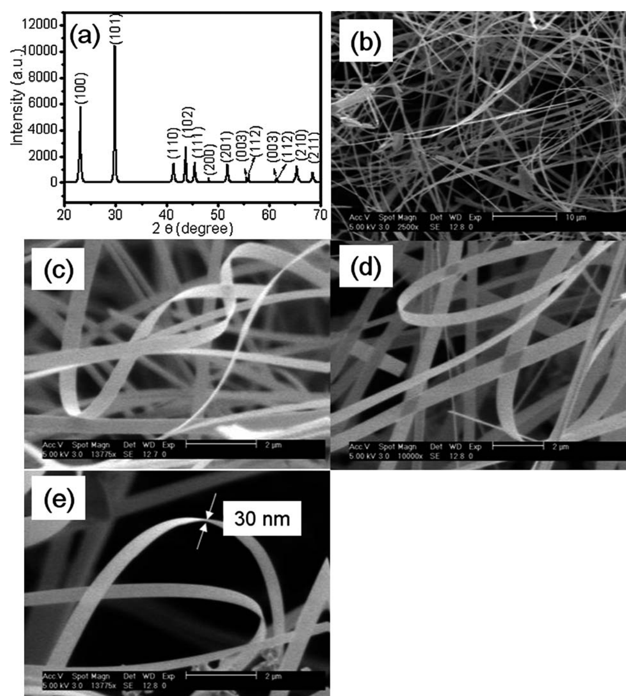

Fig. 1 (a) XRD pattern of the as-prepared *t*-SeNBs. (b) SEM image of the as-synthesized SeNBs at low magnification. (c), (d) and (e) SEM images of the SeNBs at high magnification.

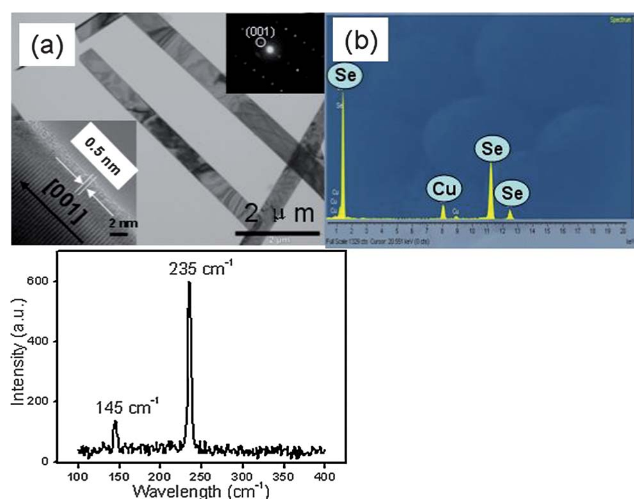

Fig. 2 (a) TEM image of the SeNBs, the corresponding SAED pattern and HRTEM image is shown in the right and left insets, respectively. Note that the length of the NB is long the [001] direction, and the fringe spacing of 0.5 nm corresponds to the (001) lattice spacing of trigonal selenium. (b) EDX analysis of the SeNBs. (c) μ-Raman spectrum of the as-prepared SeNBs.

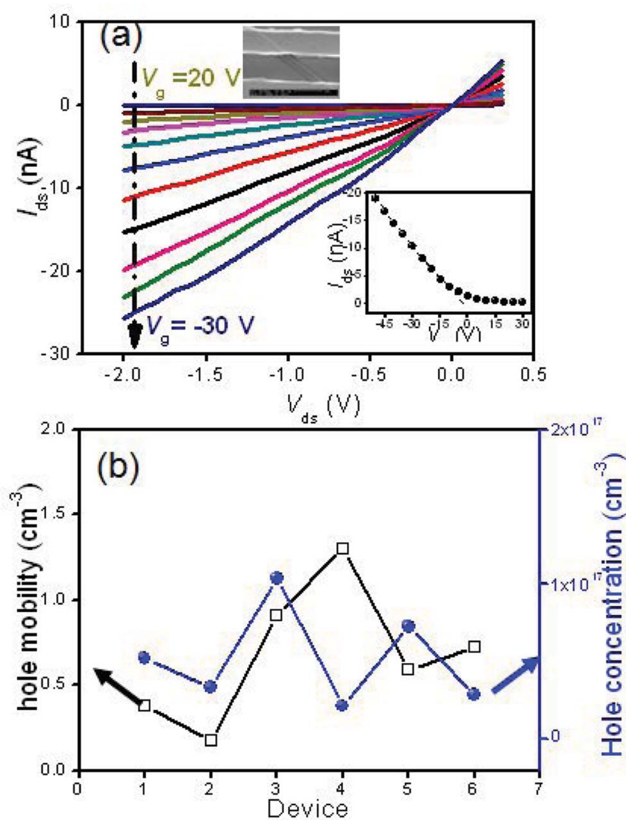

Fig. 3 (a) The family of I_{ds}–V_{ds} curves of a representative SeNB-FET at different V_g (gate voltage step is 5 V), the upper inset shows the SEM image of a typical SeNB-FET, the lower inset shows the I_{ds}–V_{gs} curve at V_{ds}= −0.5 V. (b) Hole mobility and concentration distribution of six representative SeNB-FETs.

increasing V_{gs}, suggesting typical p-type conduction characteristics. The hole mobility (μ_h) of the device can be determined by using the equation: $\mu_h = g_m L/ZC_\sigma V_{ds}$ in the linear region of I_{ds}–V_{gs} curves,[16,17] where $g_m = dI_{ds}/dV_{ds}$ is the linear-region channel transconductance, C_σ is the capacitance of the back gate, Z/L is the width-to-length ratio of the channel. The capacitance can be given by $C_\sigma = \varepsilon_r\varepsilon_0/h$, where ε_r is the dielectric constant for SiO_2 layer (3.9), ε_0 the vacuum permittivity (8.85 × 10^{-14} F cm^{-1}), and h the thickness of the SiO_2 layer (500 nm). Based on the above constants and equations, hole mobility is calculated to be 0.63 cm^2 (V $s)^{-1}$. Additionally, The hole concentration (n_h) is estimated to be 9.35 × 10^{16} cm^{-3} from the relation of $n_h = 1/\rho q \mu_h$, where ρ (the resistivity of the SeNB) is 105.6 Ωcm, and q is elementary charge (1.6 × 10^{-19} C). The reproducibility was studied *via* similar FET analysis on 6 SeNBs. As shown in Fig. 3(b), most of the SeNBs show a mobility in the range of 0.3–1.4 cm^2 (V $s)^{-1}$ with an average value of 0.67 cm^2 (V $s)^{-1}$ (Fig. 3(b)). Such a value is about 1–2 orders of magnitude larger than that obtained from solution method.[18] This improvement is undoubtedly due to the reduced density of trapping centers, as a consequence of improved crystallization at a relatively high growth temperature.[19]

Though undoped thin film or Se nanostructures have long been known to exhibit p-type electrical conduction,[18,20] the exact reason behind this phenomenon remains unclear thus far. To unveil the origin of the extrinsic characteristics, a pure SeNW without any group termination or surface adsorption was firstly considered (Fig. 4(a)). Theoretical results show that it is a virtually intrinsic semiconductor as the corresponding electronic structure does not display any defect level within the band structures (Fig. 4(e)). Owing to the relatively active reactivity at 250 °C, Se atoms on the NWs surface are apt to get contaminated, leading to the formation of different terminations on the NW surface. In light of this, the influence of surface termination (such as H-, OH-, O-) on the electrical property of SeNW was examined as well. Fig. 4(f) and (g) respectively show the electronic structures of a hydrogen and hydroxyl-terminated SeNWs, in which two defect levels were generated slightly above valence band maximum (VBM). The defect energy level (E_d) is 0.42/0.43 eV above the VBM and 0.93/1.03 eV below the conduction band minimum (CBM) in H–/OH–terminated SeNW. These defect energies imply that it is much easier for electrons to be drawn from the VBM than to be released into the CBM. Thus H- and OH- termination would produce holes, rendering SeNWs p-type conducting. It is worth mentioning that when the H-/OH- is replaced with an O atom, the defect level will shift from the VBM to the CBM, making the system have an n-type character discrepancy in electrical conduction further consolidates the important roles surface terminations play in determining the electrical conductivity of SeNBs.

The as-prepared SeNBs were then used as building units to construct a transparent and flexible photodetector. To increase light transmittance, a ITO thin layer was used as the electrode material. Fig. 5(a) displays a representative schematic illustration of the SeNB photodetector assembled on a PET substrate in which two parallel ITO electrodes are bridged by a single SeNB. The pure PET film exhibits over 90% optical transmittance in the visible range (Fig. 5(b)). Notably, after device fabrication, the transmittance decreases a little bit, over 85% in majority of

Published on 23 January 2012. Downloaded by HeFei University of Technology on 18/10/2015 13:16:02.

 This journal is © The Royal Society of Chemistry 2012

Published on 23 January 2012. Downloaded by HeFei University of Technology on 18/10/2015 13:16:02.

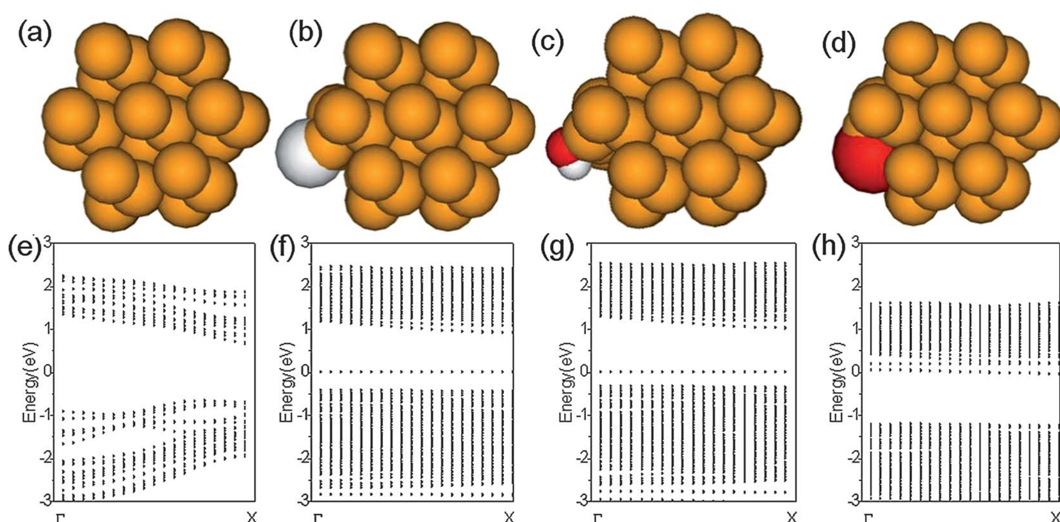

Fig. 4 (a), (b), (c) and (d) The geometries of pure SeNW, H-, OH- and O-terminated [100] oriented SeNW with a hexagon cross-section, respectively. (e), (f), (g) and (h) Band structures for (a), (b), (c) and (d), respectively. Orange spheres denote Se atoms, while red and white spheres respectively represent O and H atoms.

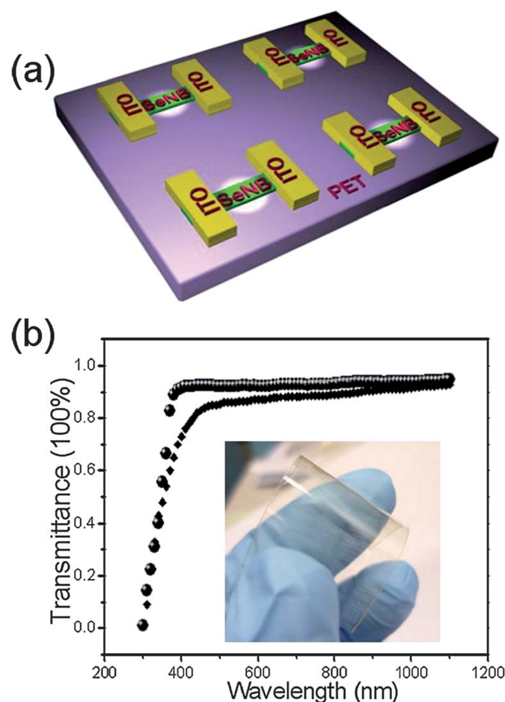

Fig. 5 (a) Schematic illustration of the SeNB photodetectors on transparent and flexible PET film, (b) optical transmittance spectra of both naked PET (sphere) and PET after devices fabrication (square), the inset shows a typical digital cameral picture of the photodetectors on PET film.

the visible range. The slight transmittance loss is reasonably due to the light absorption of both SeNBs and ITO thin film.

The SeNB photodetector exhibits high sensitivity to photon irradiation. Fig. 6(a) compares the *I–V* curves with and without light illumination. The current in the dark is 0.672 nA around at $V_{bis} = 3$ V, but increases by nearly 3 orders of magnitude to 916 nA when exposed to light illumination with a wavelength of 600 nm. The non-linear *I–V* curve is likely due to the formation of a Schottky barrier between the ITO electrode and SeNB. The time response of NB photodetector is shown in Fig. 6(b), which is measured by periodically turning on and off a light. Clearly, the nanodevice shows reversible switching between low and high conductance states with good stability and reproducibility. To assess the electrical output per optical input of the SeNB photodetector, both responsivity (R) and photoconductive gain (G) are calculated. The responsivity can be determined from the equation:[21] $R = I_p/P_{opt} = \eta\lambda q/hcG$, where I_p is the photocurrent (916 nA), P_{opt} is the incident light power (2.8×10^{-11} W), $\lambda$is the incident light wavelength (600 nm), h is Planck's constant, c is the light velocity, and η is the quantum efficiency which is assumed to be 1 for simplicity. Based on the above values, the responsivity is derived to be 3.27×10^4 A W^{-1}.

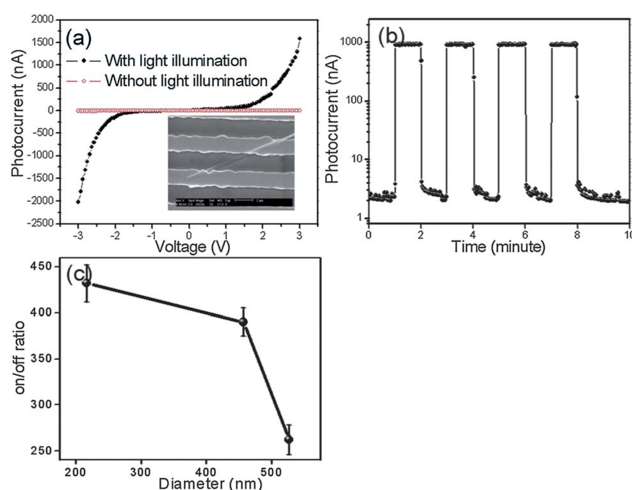

Fig. 6 (a) *I–V* curve of an individual SeNB based photodetector with and without light illumination; the inset shows a typical SEM image of the photodetector. (b) Photoresponse of the device without light switched on and off repeatedly. The light wavelength and light intensity are 600 nm and 2 mW cm^{-2} respectively. (c) On–off ratio *vs.* width of the SeNBs.

Published on 23 January 2012. Downloaded by HeFei University of Technology on 18/10/2015 13:16:02.

What is more, the photoconductive gain is estimated to be 6.77×10^4. These two parameters are comparable to those measured on chlorine doped ZnS nanowires,[21] but much higher than GaN[22] and ZnO nanowires.[23] The high quality of SeNB and the Schottky contact between the SeNB and electrodes are considered important to this relatively high responsivity and photoconductive gain. It should be noted that the photosensitivity is highly dependent on the width of the SeNBs. Fig. 6(c) summaries the current ratio *vs.* width of SeNB, from which, the on–off ratios are observed to decrease with the increase of the width. The higher surface-to-volume ratio and lower contact resistance are possibly responsible for such width-dependent photosensitivity.[24]

Next, the spectral photoresponse of the photodetector is investigated to evaluate its selectivity. Fig. 7 plots the normalized sensitivity of the SeNB device and the absorption spectrum as a function of light wavelength. It is noted that the sensitivity of SeNB is rather low for the light with a wavelength longer than 750 nm. When the wavelength is shorter than 750 nm, the sensitivity enhances sharply and reaches a peak value at a wavelength of ~480 nm. The cutoff energy is slightly smaller than the band gap of SeNBs, which is due to the presence of band-edge defects in the SeNBs. Further energy enhancement in incident light (shortening in wavelength), however, cause a drop in sensitivity. This drop in sensitivity to photon with higher energy may be regarded as a consequence of enhanced photo absorption and shortened lifetime of the electron-hole pairs at or near the surface region of the SeNBs.[25]

In addition to the good selectivity, the photodetector constructed on a flexible PET film can allow effective photodetection under various bending conditions. Fig. 8 plots the *I–V* characteristics of the SeNB photodetector exposed to pulsed light illumination with different bending angles. Obviously, the device shows excellent reproducibility and stability before and after bending the PET substrate to angles of 15 and 30° relative to the horizontal level. What is more, Both the rise and fall times are estimated to be 0.57/2.65, 0.56/2.66, 0.56/2.67 ms, for 0, 15 and 30° bending, respectively, such a feature suggests that the current SeNB photodetector can work at various bending conditions, which is of paramount significance to the future semiconductor nanostructures based optoelectronics.

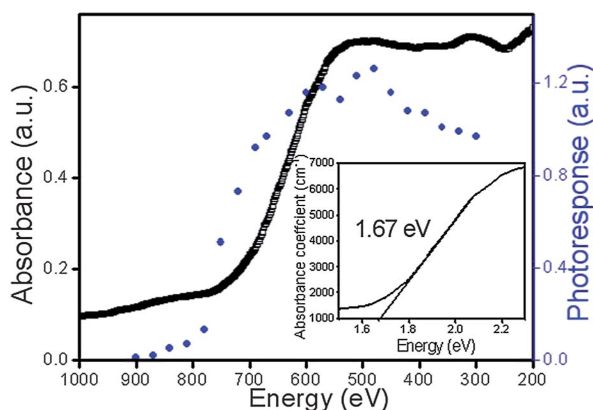

Fig. 7 Spectral response of the SeNB-based photodetector at a bias of 3 V (blue sphere), and UV-vis absorption spectrum of the SeNBs dispersed in alcohol (black square). The inset shows the bandgap determined by plotting the absorption coefficient against the energy of the incident light.

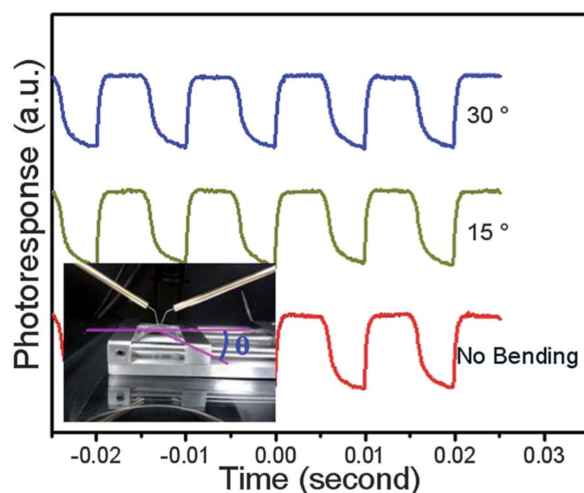

Fig. 8 Photoresponse of the photodetector a PET substrate with different bending angles: 0, 15 and 30°, the frequency of the pulsed light is set at 100 Hz by using a rotary chop during measurement. The inset shows a typical cameral picture of the bending setup.

Conclusions

In summary, we have demonstrated a new approach for the effective fabrication of [001] oriented SeNB *via* simple vacuum evaporation. Field effect transistor device made of the as-prepared SeNB exhibits typical p-type conduction characteristics, with a hole mobility and concentration of 0.63 $cm^2 (V s)^{-1}$ and 9.35×10^{16} cm^{-3}, respectively. According to our theoretical simulation, the accumulation of hole gas in the SeNB can be attributed to hydrogen and hydroxyl-termination. Photoconductivity analysis of the SeNB based photodetector shows high sensitivity to visible light illumination. The responsivity and photoconductive gain are estimated to be 3.27×10^4 A W^{-1} and 6.77×10^4, respectively. Finally, the device can work under various bending conditions with excellent reproducibility and stable performance. The totality of the above results suggests that the p-type SeNBs obtained *via* thermal evaporation are promising building blocks for future nano-optoelectronic devices.

Acknowledgements

The authors thank Mr. Ming Qiu (PhD candidate) at Department of Building Construction, City University of Hong Kong for helpful discussion. This work was supported by the National Natural Science Foundation of China (Nos. 60806028, 61106010, 21101051, 20901021,1104080), the Program for New Century Excellent Talents in University of the Chinese Ministry of Education (NCET-08-0764), the Major Research Plan of the National Natural Science Foundation of China (No. 91027021), and the Fundamental Research Funds for the Central Universities (No.2011ZM0090).

References

1 WHO working group, *Environ. Health Criter.*, 1987, **58**, 306.
2 L. I. Berger, *Semiconductor Materials*, CRC Press, Boca Raton, FL 1997, pp.86–88.

This journal is © The Royal Society of Chemistry 2012

Published on 23 January 2012. Downloaded by HeFei University of Technology on 18/10/2015 13:16:02.

3 B. Gates, B. Mayers, A. Grossman and Y. N. Xia, *Adv. Mater.*, 2002, **14**, 1749.
4 Y. N. Xia, P. D. Yang, Y. G. Sun, Y. Y. Wu, B. Mayers, B. Gates, Y. D. Yin, F. Kim and Y. Q. Yan, *Adv. Mater.*, 2003, **15**, 353.
5 B. Gate, Y. D. Yin and Y. N. Xia, *J. Am. Chem. Soc.*, 2000, **122**, 12582.
6 Q. Y. Lu, F. Gao and S. Komarneni, *Chem. Mater.*, 2006, **18**, 159.
7 L. P. Liu, Q. Peng and Y. D. Li, *Nano Res.*, 2008, **1**, 403.
8 Q. Xie, Z. Dai, W. W. Huang, W. Zhang, D. K. Ma, X. K. Hu and Y. T. Qian, *Cryst. Growth Des.*, 2006, **6**, 1514.
9 L. B. Luo, J. S. Jie, Z. H. Chen, X. J. Zhang, X. Fan, G. D. Yuan, Z. B. He, W. F. Zhang, W. J. Zhang and S. T. Lee, *J. Nanosci. Nanotechnol.*, 2009, **9**, 6292.
10 P. Liu, Y. R. Ma, W. W. Cai, Z. Z. Wang, J. Wang, L. M. Qi and D. M. Chen, *Nanotechnology*, 2007, **18**, 205704.
11 M. H. Chen and L. Gao, *Chem. Phys. Lett.*, 2006, **417**, 132.
12 H. Zhang, M. Zuo, S. Tan, G. P. Li, S. Y. Zhang and J. G. Hou, *J. Phys. Chem. B*, 2005, **109**, 10653.
13 Q. Wang, G. D. Li, Y. L. Liu, S. Xu, K. J. Wang and J. S. Chen, *J. Phys. Chem. C*, 2007, **111**, 12926.
14 X. M. Li, Y. Li, S. Q. Li, W. W. Zhou, H. B. Chu, W. Chen, I. L. Li and Z. K. Tang, *Cryst. Growth Des.*, 2005, **5**, 911.
15 C. H. An and S. T. Wang, *Mater. Chem. Phys.*, 2007, **101**, 357.
16 J. S. Jie, W. J. Zhang, Y. Jiang and S. T. Lee, *Appl. Phys. Lett.*, 2006, **89**, 223117.
17 S. M. Sze, *Physics of Semiconductor Devices*, Wiley, New York, 2nd edn, 1981.
18 Z. M. Liao, C. Hou, Q. Zhao, L. P. Liu and D. P. Yu, *Appl. Phys. Lett.*, 2009, **95**, 093104.
19 J. S. Jie, W. J. Zhang, K. Q. Peng, G. D. Yuan, C. S. Lee and S. T. Lee, *Adv. Funct. Mater.*, 2008, **18**, 3251.
20 T. Ogino, A. Takeda, Y. Mizushima, M. Oka and H. Ito, *Jpn. J. Appl. Phys.*, 1984, **23**, 639.
21 Y. Q. Yu, J. S. Jie, Q. Jiang, L. Wang, C. Y. Wu, Q. Peng, X. W. Zhang, Z. Wang, C. Xie, D. Wu and Y. Jiang, *J. Mater. Chem.*, 2011, **21**, 12632.
22 R. S. Chen, H. Y. Chen, C. Y. Lu, K. H. Chen, C. P. Chen, L. C. Chen and Y. J. Yang, *Appl. Phys. Lett.*, 2007, **91**, 223106.
23 Y. K. Su, S. M. Peng, L. W. Ji, C. Z. Wu, W. B. Cheng and C. H. Liu, *Langmuir*, 2010, **26**, 603.
24 X. J. Zhang, J. S. Jie, W. F. Zhang, C. Y. Zhang, L. B. Luo, Z. B. He, X. H. Zhang, W. J. Zhang, C. S. Lee and S. T. Lee, *Adv. Mater.*, 2008, **20**, 2427.
25 L. B. Luo, F. X. Liang and J. S. Jie, *Nanotechnology*, 2011, **22**, 485701.

This journal is © The Royal Society of Chemistry 2012